Pollen Patterns Form from Modulated Phases

Asja Radja[1], Eric M. Horsley[1], Maxim O. Lavrentovich[2*], and Alison M. Sweeney[1*]

asjar@sas.upenn.edu
ehorsley@sas.upenn.edu
*mlavrent@utk.edu
*alisonsw@sas.upenn.edu

[1]Department of Physics and Astronomy, University of Pennsylvania, 209 S. 33rd St., Philadelphia, Pennsylvania 19104, U.S.A.

[2]Department of Physics and Astronomy, University of Tennessee, 1408 Circle Dr., Knoxville, Tennessee 37996, U.S.A

*Co-corresponding authors

Abstract

Pollen grains are known for their impressive variety of species-specific, microscale surface patterning. Despite having similar biological developmental steps, pollen grain surface features are remarkably geometrically varied. Previous work suggests that a physical process may drive this pattern formation and that the observed diversity of patterns can be explained by viewing pollen pattern development as a phase transition to a spatially modulated phase. Several studies have shown that the polysaccharide material of plant cell walls undergoes phase separation in the absence of cross-linking stabilizers of the mixed phase. Here we show experimental evidence that phase separation of the extracellular polysaccharide material (primexine) during pollen cell development leads to a spatially modulated phase. The spatial pattern of this phase-separated primexine is also mechanically coupled to the undulation of the pollen cell membrane. The resulting patterned pools of denser primexine form the negative template of the ultimate sites of sporopollenin deposition, leading to the final micropattern observed in the mature pollen. We then present a general physical model of pattern formation via modulated phases. Using analytical and numerical techniques, we find that most of the pollen micropatterns observed in biological evolution could result from a physical process of modulated phases. However, an analysis of the relative rates of transitions from states that are equilibrated to or from states that are not equilibrated suggests that while equilibrium states of this process have occurred throughout evolutionary history, there has been no particular evolutionary selection for symmetric, equilibrated states.

Introduction

The diversity and beauty of pollen grain surface patterns have intrigued scientists for decades, yet no unifying theory has emerged to explain either the pattern formation mechanism or the function of these surface features (Fig. 1)[1]. So, a natural question is: how do pollen grains create such diverse, microscale patterns when other cells typically do not? Has there been evolutionary selection for symmetric patterns, or are these patterns the result of evolutionary drift of a separate biochemical process? Geometrically similar patterns are found on fungal spores, mite carapaces, and insect eggs, but these patterns are not nearly as diverse as those found on pollen[2]. The multitude of pollen patterns observed in nature, along with a complex extracellular composition, make understanding pollen development particularly difficult. Our objective is to provide a unified conceptual framework for understanding the patterning process.

In mature pollen, the outermost layer of the extracellular material is highly patterned and called the exine. The exine is a chemically and physically robust outer wall made of sporopollenin, a complex, highly resistant chemical whose structure and composition are not fully described[3]. Apart from the structure of the exine itself, pollen can be patterned with a varying number and geometric arrangement of apertures, which are regions of the extracellular material that have a reduced or absent exine and are the sites where the pollen tube emerges during germination[4]. Apertures also allow the pollen grain to reversibly fold during desiccation and rehydration[5].
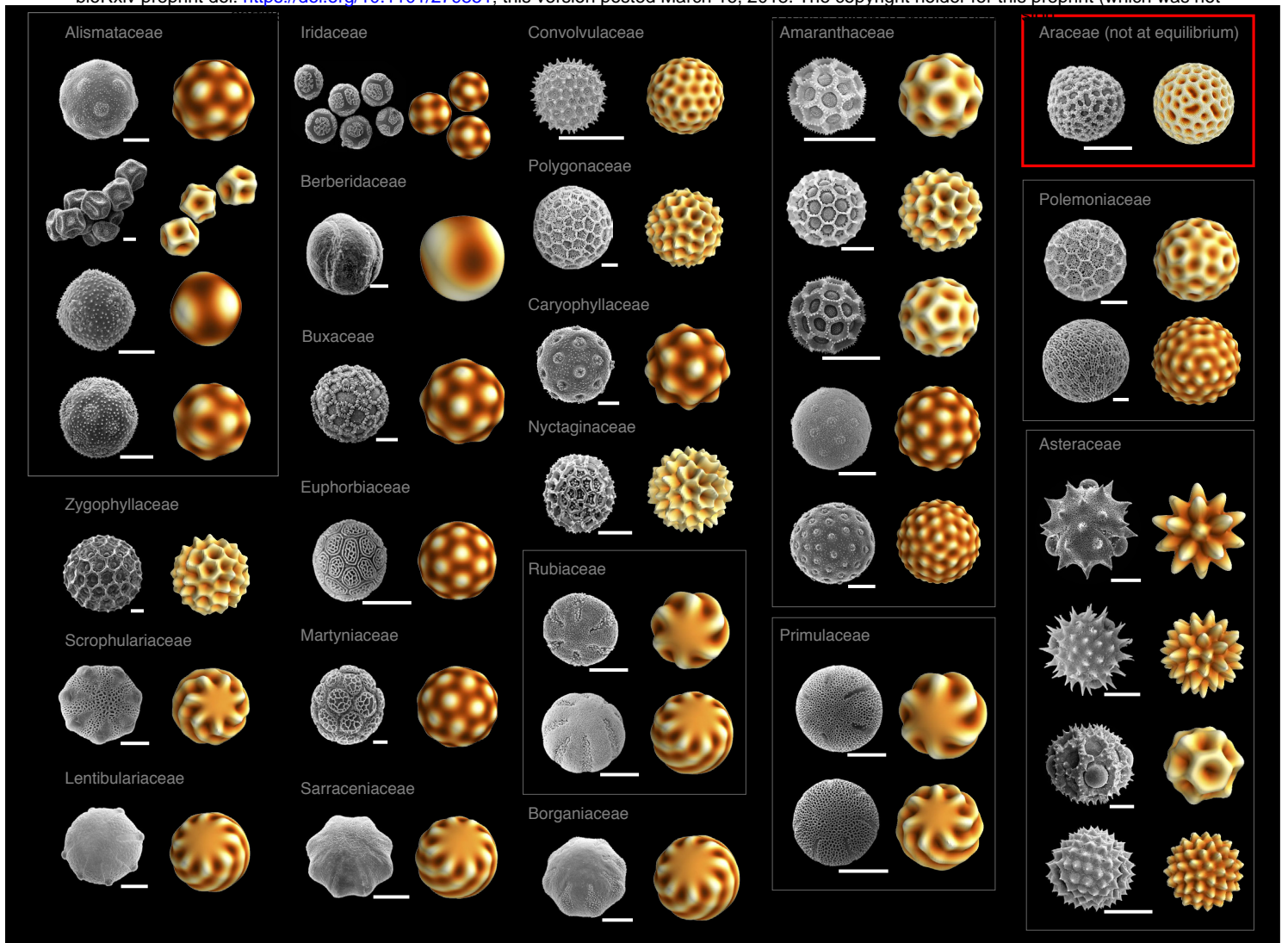
Figure 1: Pollen SEMs and recapitulated patterns. Pairs of images illustrate examples of pollen grain surface patterns reproduced with our simulations. These selected pairs represent examples of the range of patterns we found at equilibrium patterns (polygonal spikes, polygonal holes, chiral stripes, and mixtures of these); the red box represents an example of non-equilibrium patterns that are mostly foamy (reticulate). The left image in each pair shows the SEM of a given species, the right image in each pair shows the simulated surface of the same geometry. The species represented and the Hamiltonian parameters (l_0, λ'_3) producing the matching simulated surface are listed. All SEM micrographs from paldat.org; all equilibrium simulations used $(R^2 \tau)/K = -1$. **First column:** *Alisma lanceolatum*, (9.5,1); *Caldesia parnassifolia*, (5.5,-1); *Echinodorus cordifolius*, (4.5,1); *Echinodorus quadricostatus*, (7.5,1); *Kallstroemia maxima*, (16.5,-1); *Diascia barberae*, (12.5,0); *Utricularia sandersonii*, (13.5,0). **Second column:** *Iris bucharica*, (6.5,1); *Berberis vulgaris*, (3.5,0); *Sarcococca hookeriana*, (9.5,1); *Phyllanthus sp.*, (11.5,1); *Ibicella lutea*, (11.5,1); *Sarracenia flava*, (13.5,0). **Third column:** *Ipomoea cholulensis*, (19.5,-1); *Persicaria mitis*, (19.5,-1); *Cerastium tomentosum*, (9.5,1); *Bougainvillea sp.* (17.5,-1); *Galium wirtgenii*, (8.5,0); *Galium album*, (13.5,0); *Arnebia pulchra*, (13.5,0). **Fourth column:** *Pfaffia gnaphaloides*, (10,-1); *Gomphrena globosa* (15.5,-1); *Pfaffia tuberosa*, (12,-1); *Amaranthus blitum*, (12.5,1); *Chenopodium album*, (19.5,1); *Primula veris*, (8.5,0); *Primula elatior*, (12.5,0). **Fifth column:** (red box) *Anthurium gracile*, simulated with conserved dynamics [Eq. (7) with $D=K=1, q_0=1.5, \tau=-20, \lambda_3=-20, \lambda_4=120$, and a sphere radius of $R=15$, for dimensionless parameters $l_0=22.5, \lambda_3 \approx -27.4, (R^2 \tau)/K=-4500$. We used a Gaussian, random initial $\psi(\theta, \varphi)$ centered around 0 with a variance of 0.04, and evolved the field until time t=2]; *Phlox drummondii*, (16.5,-1); *Polemonium pauciflorum*, (20.5,1); *Gaillardia aristata*, (10,1); *Bidens pilosa*, (14.5,1); *Chondrilla juncea*, (8,-1); and *Iva xanthiifolia*, (19.5,1).

41   The general developmental steps that result in the observed variety of pollen surface
42   patterns are well-characterized[6]. The cell wall of the meiotic mother cell fails to completely
43   divide, leaving the resulting daughter pollen cells contained within a specialized structure called
44   the callose wall, and, as a result, they are isolated from the rest of the anther fluid. The callose
45   wall has an unusual composition of β-1,3 glucan, which provides an experimental strategy for its
46   selective degradation to access the developing pollen grains[7]. The developing pollen cells then

47   secrete a polysaccharide material called the "primexine" to the cell surface; the primexine

48   accumulates between the cell's plasma membrane and the callose wall. The composition of the

49   primexine is not well-characterized but is likely to be a high molecular weight polysaccharide[8]. It

50   has been established that the global pattern features of the mature pollen wall (exine) are

51   somehow templated by the developing primexine layer during this enclosed "tetrad" stage[8,9,10],

52   though the physical mechanism of this process remains undescribed. Following this global

53   templating by the primexine, the callose wall dissolves and sporopollenin is secreted by adjacent

54   tapetal cells and accumulates on the pollen cell surface, resulting in the patterned exine layer of

55   mature pollen (Fig. 1).

56   Several studies suggest that pollen apertures may also be features dictated by the

57   primexine process, especially in multi-aperturate and spiraperturate pollen[11,12]. However, in

58   pollen grains that contain fewer than six apertures, the aperture pattern may be established by

59   points of cellular contact between daughter cells during meiosis[13]; since apertures possibly

60   arising by this mechanism have a tetrad geometry of daughter cells, they are easy to identify, and

61   we excluded them from this analysis of pattern formation via a primexine template. It is clear

62   that there is no one unified cell developmental mechanism of aperture formation across plants[11];

63   therefore, we adopt the definition that apertures are simply thin regions of the exine material.

64   Here, we provide a physical explanation for the generation of the templated pattern by the

65   primexine material.

66   A physical theory for cell surface patterning via a first-order phase transition of material

67   deposited on the cell surface was recently reported by Lavrentovich and colleagues[14]. Here we

68   treat the primexine as a phase-separating concentration field on a spherical surface, which in turn

69   introduces heterogeneities (e.g., a locally varying pressure or preferred curvature) and a local

70   buckling of the plasma membrane. Such heterogeneities, when coupled to the elasticity of a

71   membrane, are known to create spatially modulated structures[15]. In pollen, a mechanical

72   coupling between the polysaccharide matrix and membrane may be promoted by the presence of

73   the outer callose wall that encapsulates extracellular polysaccharides near the cell membrane

74   during pattern formation. Initial pattern formation could then occur via a phase transition of the

75   polysaccharide to a spatially modulated state. The same kind of transition has been used to

76   describe the formation of viruses[16,17] and two-component vesicles[18,19], which are also intricately

77   patterned spherical objects, and discretized versions of such patterned spherical objects have also

78   been computationally explored[20]. We employ a fully spectral method that allows for a systematic

79   characterization of pattern configurations.

80   In addition to the pollen pattern formation process being unknown, there has been no

81   unifying, satisfactory answer to what the functional role of these patterns might be, in spite of

82   many previous efforts. Some studies have found a correlation between pollinator types and

83   pollen grain surface features[21]. Other studies have found that there is a general trend of

84   increasing aperture number in angiosperms[22]. However, the findings of these studies often

85   conflict, and there is no current consensus as to which features of pollen patterns may be

86   evolutionarily selected for and why.

87   We show that the preponderance of extant pollen patterns can be explained through a
88 phase transition of the primexine coupled to the plasma membrane during cell development. We
89 also show novel experimental corroboration of a densification and pooling of primexine material
90 leading to membrane undulations at the wavelength of the mature pollen pattern in *Passiflora*
91 *incarnata*, a species whose exine is reticulate (foamy). This mechanism implies that evolutionary
92 pattern diversity is to be expected, given the general chemical composition and physical makeup
93 of the pollen grain during development and that the spherical surface of pollen grains must
94 accommodate spherical defects in the resulting pattern. Further, most of the ordered states
95 observed in evolved pollen pattern diversity can be recapitulated with a unique set of parameters
96 in our theory (Fig. 1). Our theory is also able to account for patterns generated by this physical
97 mechanism that do not reach an energy minimum (Fig. 1, red box). A surprise in our results is
98 that the majority of mature, extant pollen patterns do not exist at energy minima within this
99 pattern formation landscape; there apparently has been no strong evolutionary selection for
100 symmetry via pattern equilibration in pollen. Finally, we propose a new way of characterizing
101 pollen patterns motivated by this physical theory that is grounded in the physiology of pollen
102 development.
103
104 **Materials and Methods**
105 *Microscopy*
106   *Passiflora incarnata* (Shady Oak Butterfly Farm) was grown at the University of
107 Pennsylvania Department of Biology greenhouse under a 16 hour/day light cycle at a mean
108 temperature of 77°F. Fresh anthers were collected, and pollen was immediately dissected out of
109 the developing anthers within flower buds. To identify the stage of pollen development in a
110 given anther, one anther from each flower bud was pressed between glass slides and examined
111 with a brightfield optical microscope; only pollen in the tetrad stage was kept for further
112 analysis.
113   For transmission electron microscopy (TEM), anthers were first fixed in 3%
114 gluteraldehyde with 1% alcian blue in 1x phosphate-buffered saline (PBS) for 24 hours[23], and
115 then post-fixed in 2% osmium tetroxide for 30 minutes. Next, an ethanol dehydration series was
116 performed, and samples were embedded in Spurr's resin. Transverse ultrathin sections of 70 nm
117 were cut with a Diatome diamond knife on a Reichert Ultracut-S microtome. Secondary staining
118 was done with uranyl acetate and lead citrate. Sections were placed on copper mesh grids and
119 imaged with a JEOL JEM-1010 electron microscope.
120   For scanning electron microscopy (SEM), we first separated the developing tetrads from
121 their anthers and then enzymatically removed the callose walls, as described by Kirkpatrick and
122 Owen[24]. The pollen grains from a single developing flower were placed in 1mL of 0.3% w/v
123 cellulase, pectolyase and cytohelicase, 1.5% sucrose, and 1% polyvinylpyrolidone for 2 hours
124 (Sigma-Aldrich; Milwaukee, MI). Next, the pollen grains were fixed in 3% gluteraldehyde in 1x
125 PBS for 1 hour. Samples were then washed in deionized water for 5 minutes and placed in
126 handmade Nitex bags (1 cm^2); the bags were then heat sealed. The bags with the pollen samples

were then submerged in 1x PBS for 5 minutes, followed by an ethanol dehydration series. Samples were then critical-point dried in CO_2 in a Tousimi Autosamdri-850. The pollen grains were removed from the bags, placed onto SEM stubs and sputter coated with a ~10 nm thick layer of gold-palladium using an SPI Module Sputter Coater. We prepared pollen grains at the same stage without enzymatically removing the callose walls as control for any unintended effects of the removal procedure. Samples were imaged using a FEI Quanta FEG 250.

Primexine composition

Pollen grains at the tetrad stage were also collected to analyze their primexine composition. We dissected pollen grains from anthers and enzymatically removed the callose walls using the method described in the section above. The whole pollen grains (without their callose walls) were then frozen and shipped over dry ice to the Complex Carbohydrate Research Center at the University of Georgia for a glycosyl composition and linkages analysis. The monosaccharide composition and linkages analyses were performed by combined gas chromatography/mass spectrometry of the per-*O*-trimethylsilyl derivatives as described previously by Santander and colleagues[25]. More details on the method used are in the supplemental information.

Theoretical Model

We describe the formation of the pollen surface pattern as a phase separation of the primexine mechanically coupled to the underlying plasma membrane. It should be noted that we are not modeling any detailed material properties of the primexine, but we do assume that it is able to phase separate, similar to mixtures of other high molecular weight extracellular polysaccharides such as hemicellulose and pectin[26,27]. This model is described in more detail in a previous study where the effects of thermal fluctuations on patterned states were additionally considered[14]. The present work focuses on a microscopic model without these fluctuation effects to study the number, variety, and stability of ordered states (which is much more difficult to do in the fluctuating case). We will include a brief description here for clarity.

Consider a scalar field, ψ, which represents the concentration field of the primexine polysaccharides in contact with the outer surface of a pollen grain plasma membrane. We postulate that the phase separation of this material drives the pattern formation of the pollen surface. The general Landau-Ginzburg free energy for ψ is given by

$$\mathcal{H}[\psi] = \int d^2x \left[\frac{\kappa_0}{2} |\nabla\psi|^2 + \frac{\tau_0}{2}\psi^2 + \frac{\lambda_3}{3!}\psi^3 + \frac{\lambda_4}{4!}\psi^4 \right], \tag{1}$$

where κ_0 and $\lambda_{3,4}$ are constants that depend on some undefined primexine chemical or material properties. We assume that $\kappa_0, \lambda_4 > 0$, and τ_0 is a temperature-like term that is quenched below some critical value during pattern formation. Because this field sits on a spherical surface, we use spherical coordinates, $\psi = \psi(\theta, \phi)$ and our integration measure reads $\int d^2x = R^2 \int d\theta d\phi$, where $\theta \in [0, \pi]$ and $\phi \in [0, 2\pi)$. We then expand $\psi(\theta, \phi)$ in terms of spherical harmonics, $Y_l^m(\theta, \phi)$:

6

$$\psi(\theta,\phi) = \sum_{l=0}^{\infty}\sum_{m=-l}^{l} c_l^m Y_{lm}(\theta,\phi) \equiv \sum_l c_l^m Y_{lm} \tag{2}$$

164 Finally, the expansion coefficients satisfy the property $[c_l^m]^* = (-1)^m c_l^{-m}$ because the scalar

165 field ψ is real.

166 We now follow the infinite flat membrane analogue of our model studied by Leibler and

167 Andelman[15]. Non-patterned (uniform) states, $l = 0$ modes, are preferred in Eq (1). However,

168 when we couple this field, ψ, to the local membrane curvature, we observe patterned states. The

169 $l \neq 0$ modes are more energetically favorable in the coupled system since the primexine

170 concentration on the surface causes the membrane to bend and fluctuate away from a spherical

171 shape. Details of the implementation of this coupling are described in the work done by

172 Lavrentovich and colleagues[14]. The salient physical feature of coupling the primexine to the cell

173 membrane in this study is that a spatially modulated phase with a characteristic mode number

174 l_0 arises, which approximately describes the number of times a given pattern wraps around the

175 sphere. It is related to the characteristic wavelength, λ, by $l_0 \approx 2\pi R/\lambda$. The effective free energy

176 for the field near $l \approx l_0$ has the general form

$$\mathcal{H} = \frac{1}{2}\sum_l [K(l-l_0)^2 + R^2\tau]\,|c_l^m|^2 + \mathcal{H}_{\text{int.}} \tag{3}$$

177 where K and τ are new constants that depend on the material properties of the primexine and

178 various physical parameters of the plasma membrane such as bending rigidity, surface tension,

179 elasticity and/or lipid/protein density. These parameters may also incorporate features of the

180 callose wall if the wall participates in inducing the membrane buckling. The terms in $\mathcal{H}_{\text{int.}}$ are

181 inherited from Eq. (1) and involve couplings between different spherical harmonics:

$$\mathcal{H}_{\text{int.}} = \frac{R^2\lambda_3}{3!}\Upsilon_{m_1,m_2,m_3}^{l_1,l_2,l_3} c_{l_1}^{m_1} c_{l_2}^{m_2} c_{l_3}^{m_3} + \frac{R^2\lambda_4}{4!}\Upsilon_{m_1,m_2,\overline{m}}^{l_1,l_2,\overline{l}}\Upsilon_{m_3,m_4,-\overline{m}}^{l_3,l_4,\overline{l}} c_{l_1}^{m_1} c_{l_2}^{m_2} c_{l_3}^{m_3} c_{l_4}^{m_4} \tag{4}$$

182 where the Υs are Gaunt coefficients, with sums implied on all indices. Written in terms of the

183 Wigner-3j symbols[28], the Gaunt coefficients are given by

184

$$\Upsilon_{m_1,m_2,m_3}^{l_1,l_2,l_3} \equiv \sqrt{\frac{\prod_{i=1}^{3}(2l_i+1)}{4\pi}}\begin{pmatrix} l_1 & l_2 & l_3 \\ 0 & 0 & 0 \end{pmatrix}\begin{pmatrix} l_1 & l_2 & l_3 \\ m_1 & m_2 & m_3 \end{pmatrix}. \tag{5}$$

185 Rapid evaluation algorithms are available for these symbols[29] that we will use for calculations of

186 the minimal energy states described below.

187 We choose our units of energy, concentration, and length to reduce the Hamiltonian to

188 the form

$$\mathcal{H} = \frac{1}{2}\sum_l \left[(l-l_0)^2 + \frac{R^2\tau}{K}\right]|c_l^m|^2 + \frac{\lambda_3 R}{3!\sqrt{K\lambda_4}}\Upsilon_{m_1,m_2,m_3}^{l_1,l_2,l_3} c_{l_1}^{m_1} c_{l_2}^{m_2} c_{l_3}^{m_3}$$
$$+ \frac{1}{4!}\Upsilon_{m_1,m_2,\overline{m}}^{l_1,l_2,\overline{l}}\Upsilon_{m_3,m_4,-\overline{m}}^{l_3,l_4,\overline{l}} c_{l_1}^{m_1} c_{l_2}^{m_2} c_{l_3}^{m_3} c_{l_4}^{m_4} \tag{6}$$

189 such that we are left with three dimensionless control parameters: $l_0, \lambda_3 R/\sqrt{K\lambda_4}$, and $R^2\tau/K$.

190 For notational simplicity, we also set $\lambda_3' = \lambda_3 R/\sqrt{K\lambda_4}$.

191   The ordered (patterned) states are then a linear combination of spherical harmonic basis

192 states described by Eq. (2), where c_l^ms are the complex variables that specify the state. The

193 spherical harmonics account for the defects in the pattern induced by the spherical topology, as

194 specified by the Poincaré-Brouwer theorem[30]. We note that because we do not know the precise

195 composition of the primexine, or the effects of the callose wall or any additional chemistry in the

196 space between the cell membrane and the callose wall, the parameters of our model are by

197 necessity phenomenological. However, in principle, with a careful accounting of all the

198 chemistry of the primexine, plasma membrane, and callose wall, it would be possible to

199 independently measure the coefficients described above for a given species and pattern. Next, we

200 describe our method of exploring the phase space of ordered states by finding the set of complex

201 variables, c_l^ms, that describe the global minimum energy state.

202

203 *Phase Diagram Exploration*

204   We used simulated annealing (SA) and gradient descent (GD) methods as outlined in

205 *Numerical Recipes*[31] to solve for the minimum energy states of the Hamiltonian in Eq. (6). For

206 simplicity and analytic tractability, we used a single-mode approximation in which we consider

207 patterns at either 1) single l values where $l = l_0$ or 2) the mixing of two adjacent integer values l

208 and $l + 1$ for intermediate values of l_0 between l and $l + 1$. We also make some comments on

209 the more general case where we consider the dynamics of the pattern formation.

210   Since this free energy may potentially have many local minima for a single set of

211 parameters, we used SA to find the global minimum energy state. In this search algorithm, a

212 Metropolis criterion is used in which lower energy states in the phase space are always accepted,

213 while higher energy states are accepted with a Boltzmann probability distribution, $P \propto e^{-\Delta E/T}$,

214 given a temperature-like parameter T. The parameter T was tuned to allow the system to escape

215 local minima. Initially, T was chosen to be large enough to allow for an exploration of the whole

216 phase space; T was then lowered with a particular annealing schedule such that the system

217 settled into its global minimum as T became small[31].

218   To find the appropriate annealing schedule and number of iterations per temperature

219 value, we ran SA enough times to find consistent minimum function values at a given set of

220 parameter values for l_0 and λ_3'. We found that an optimal annealing run started with $T = 1$ and

221 an initial temperature step of $\Delta T = 0.1$. Once we reached a temperature of $T = \Delta T$, we

222 decreased our step size ΔT by a factor of 10. We continued decreasing the temperature in these

223 incrementally smaller amounts until the observed pattern no longer changed appreciably with

224 further annealing.

225   We also used GD to ensure that the SA reliably located the global energy minimum for a

226 given parameter set and to test for the presence of local minima. GD is an algorithm that

227 minimizes functions by iteratively moving in the negative direction of the function's gradient

228 until a point with a gradient of zero is found. We were able to calculate the gradient analytically

229 for our model, giving us a substantial computational speed increase.

230   To confirm the stability of the global minima found via both SA and GD, we

231 diagonalized the Hessian (matrix of second derivatives) and confirmed that all eigenvalues are

232 positive, with the exception of three zero eigenvalues corresponding to the rotations of the

233 sphere. We then comprehensively explored the phase space using both SA and GD by

234 systematically changing the parameter values, l_0 and λ'_3 , and recording the effects of those

235 changes to the pattern on the sphere surface. We set $R^2\tau/K = -1$ in this exploration of the

236 phase space to remain in the ordered state, since increasing $R^2\tau/K$ would induce a transition to

237 the unpatterned state.

238   To study the dynamics of our model, we supposed that the total volume of the primexine

239 condensed and dilute phases are fixed. Therefore, we would generally expect to find a conserved

240 dynamics for our energy. Such a dynamics, consistent with the idea that the free energy is

241 minimized by a spatial modulation with a characteristic wave number $q_0 \equiv 2\pi/\lambda$, is given by

$$\partial_t \psi(\mathbf{x}, t) = D\nabla^2 \frac{\delta\mathcal{H}}{\delta\psi} = D\nabla^2 \left[K(\nabla^2 + q_0^2)^2\psi + \tau\psi + \frac{\lambda_3}{2}\psi^2 + \frac{\lambda_4}{6}\psi^3 \right] \quad (7)$$

242 where we have slightly modified the gradient term in order to more easily integrate the equation

243 of motion. This particular equation of motion is also called the phase-field crystal model[32]. We

244 integrated Eq. (7) using the FiPy package[33], a finite volume solver. Unlike our spherical

245 harmonic method described above, this technique discretizes the sphere and does not preserve

246 rotational symmetry. In addition, we made the wavelength selection weak (i.e, allowed more

247 states away from the characteristic wavelength to contribute to the final pattern) by evolving with

248 $\tau, \lambda_{3,4} \gg K$. For a 2D flat geometry, foamy states are expected[34], and we expect a similar

249 phenomenology on the sphere.

250

251 *Evolutionary trait reconstruction*

252   To examine whether any physical features described by our model of pollen have

253 undergone evolutionary selection, we performed an evolutionary trait reconstruction and

254 subsequent analysis for relative rates of evolution between pattern types across spermatophytes

255 (seed-bearing plants). We first constructed a morphological data set for pollen surface patterns of

256 2,641 species representing 203 families using the palynology database PalDat[35]. To define a

257 tractable dataset, we limited our morphological analysis to pollen monads, though our theory is

258 potentially general enough to describe any cells of spherical topology.

259   We restricted our analysis to patterns whose development is commensurate with the

260 underlying assumptions of our model; in order to include a species, we required positive

261 documentation that during the tetrad stage, a given species exhibits plasma membrane

262 undulations with the same wavelength as the mature surface pattern. These data were gathered in

263 a comprehensive review of pollen development literature (see supplemental references). We

264 excluded from our analysis any surface features that demonstrably arise after the dissolution of

265 the callose wall (for example, most echinate spines are derived from tapetal fatty acid

266 deposition)[36]. In these cases, we ignore the post-callose-wall features and analyze the pollen
267 grain as if it did not have them.
268   We first separated all relevant PalDat SEM images into one of two categories: final
269 pattern is an equilibrium state (i.e., the observed pattern corresponded to an energy minimum
270 from our theory) and final pattern is not at an equilibrium state (i.e., the observed pattern did not
271 correspond to an energy minimum calculated from our theory; instead it was either uniform or
272 foamy). We then measured pollen pattern wavelengths manually in ImageJ. The patterns at
273 equilibrium could be identified as those with surface features with a characteristic (constant)
274 wavelength. All families with patterns in an equilibrium state also had wavelengths >3 μm,
275 except for some species in the family Amaranthaceae, which had wavelengths of 1–3 μm.
276 Conversely, patterns not at equilibrium will not demonstrate a single, constant pattern
277 wavelength but will show a range of wavelengths. Next, we further characterized patterns not at
278 equilibrium into three bins organized by their average pattern wavelength value: $\lambda < 1\mu m$,
279 $1 < \lambda < 3\mu m$, and $\lambda > 3\mu m$. Thus, we had four categories to describe pollen from a given family: (1)
280 pattern at equilibrium, $\lambda > 3\mu m$ (2) pattern not at equilibrium, $\lambda < 1\mu m$, (3) pattern not at
281 equilibrium, $1 < \lambda < 3\mu m$, (4) pattern not at equilibrium, $\lambda > 3\mu m$. Although most equilibrium
282 patterns were formed by exine features, we also considered features previously defined as
283 apertures (i.e., thin regions in the exine) with distinct characteristic wavelengths as equilibrium
284 states. We ignored apertures in a tetrahedral arrangement since these features plausibly result
285 from the geometry of meiosis rather than from the primexine[11]; we analyzed these pollen grains
286 as though the apertures were absent. The observed states not at equilibrium were often foamy
287 (reticulate) with a range of wavelengths. The smallest wavelength category ($\lambda < 1$ μm) includes
288 smooth-surfaced pollen.
289   We used a time-calibrated family-level phylogenetic tree of spermatophytes[37] identified
290 in the integrated Tree of Life (iToL) database[38] to estimate the evolutionary history of these
291 pollen pattern categories. We assigned states to the terminal nodes representing spermatophyte
292 families according to the pattern categories described above; the number of states present in a
293 single family ranged from one to the maximum of four. The Nexus file describing this tree and a
294 fully detailed tree figure are available in the supplemental data.
295   We used ancestral reconstruction, as implemented in BayesTraits[39] to study the character
296 evolution of patterned states. We used a maximum likelihood algorithm and the multistate
297 model of evolution[40]. We first tested the hypothesis that there is directional evolution either to or
298 from pollen patterns at equilibrium to those that are not at equilibrium. To do this, we defined
299 state A to be category (1), or "at equilibrium," and state B to be categories (2)–(4), or "not at
300 equilibrium". This model is called the "2-state equilibrium model".
301   We also tested whether there was directional selection for larger pattern wavelengths and
302 therefore more distinctly patterned, polygonal pollen over evolutionary time. For this test, we
303 defined three states (C, D, and E), one for each of the three wavelength categories described
304 above. State C included categories (1) and (2) for all patterns with $\lambda > 3\mu m$. State D included all
305 patterns in category (3) not at equilibrium patterns, $1 < \lambda < 3\mu m$. State E included all patterns in

10

306 category (4) not at equilibrium patterns, $\lambda < 1\mu m$. This model is called the "3-state wavelength
307 model".

Results

Microscopy

310 We divided the developmental trajectory of pollen in the tetrad state into six distinct
311 stages. In the first stage, after meiosis but before primexine secretion, the plasma membrane did
312 not undulate, there was little or no extracellular material present, and the cell surface was smooth
313 over length scales of about a micron (Fig. 2, col. 1). In the second stage, we observed the
314 primexine material appear on the cell surface (Fig. 2, col. 2, arrowhead). This material was
315 initially uniform in electron density, and the plasma membrane underneath became more
316 irregular, apparently in response to the presence of the material on the cell surface, but there was
317 not a characteristic wavelength in the membrane; the SEM of this developmental stage shows the
318 appearance of a dough-like material on the surface of the cell (Fig. 2, col. 2). In the third stage,
319 the primexine began developing heterogeneities in electron density, and the corresponding SEM
320 showed clumping of the surface material into regions of ~0.5 μm in width, but there was still no
321 characteristic wavelength in the membrane undulation (Fig. 2, col. 3). In the fourth stage, the
322 primexine heterogeneities became more pronounced and the plasma membrane began to
323 undulate with a characteristic wavelength; the SEM at this stage shows distinct domains of
324 separated primexine material on the cell surface with regions of positive curvature separating
325 these domains (Fig. 2, col. 4).
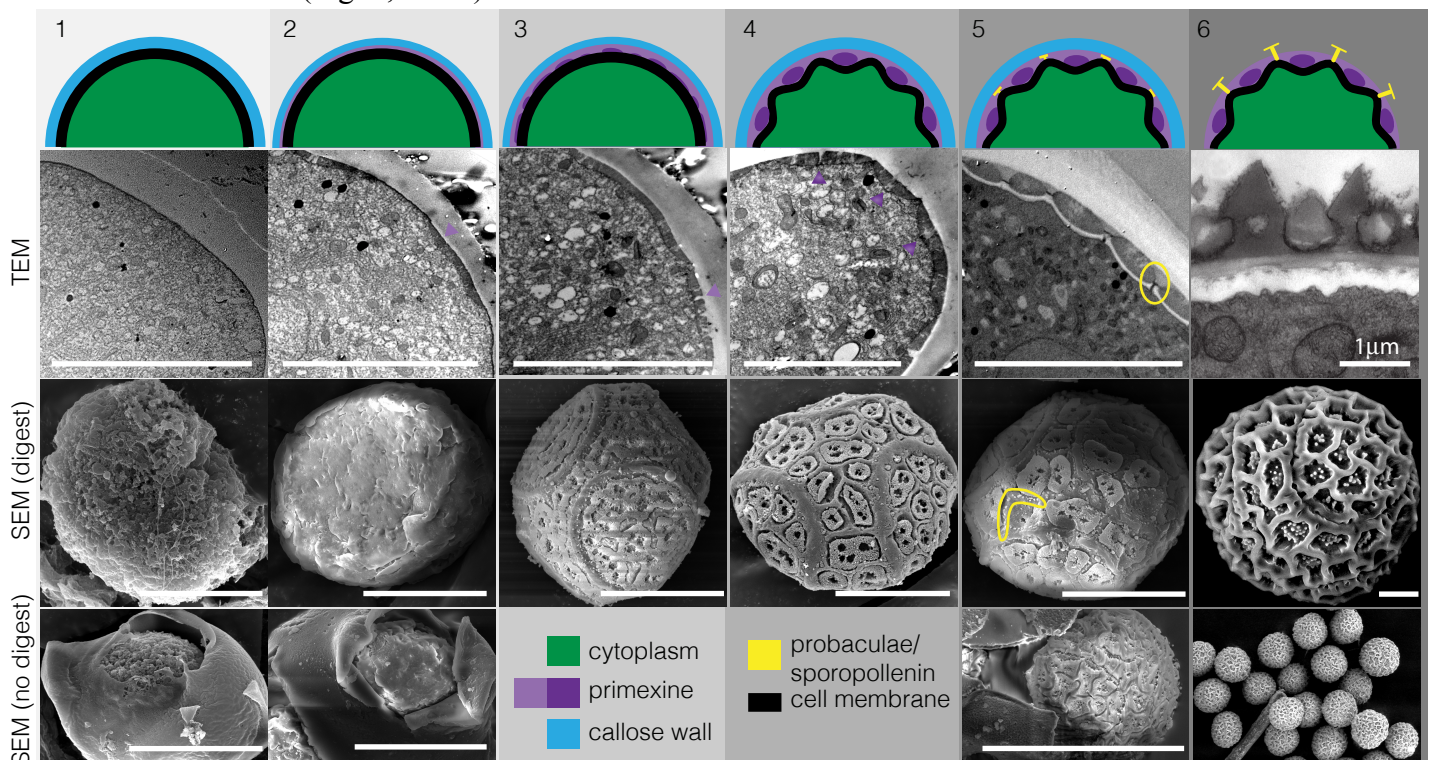
Figure 2: *Passiflora incarnata* primexine phase separation. We define five developmental steps of pattern formation occurring after meiosis and prior to callose wall dissolution; the sixth step represents mature pollen. Development proceeds left to right. The first row contains a schematic representation of each step. The second row shows TEM images, the third row shows SEM images with the callose wall enzymatically removed, and the fourth row shows SEM images where the callose wall was mechanically opened but not enzymatically removed. In general, the surface of developing pollen is similar whether the callose wall was removed enzymatically or mechanically. Arrowheads in column 2 indicate the location of the primexine on the cell membrane surface. Arrowheads in columns 4 and 5 indicate the location of dense primexine that causes the cell membrane to locally curve. The circle in column 5 highlights initial formation of probacula/sites of sporopollenin deposition. All scale bars represent 10 *μm*.

11

326   In the fifth stage, the phase separation of primexine was complete, with two
327 geometrically regular materials of distinctly different density in contact with the cell
328 membrane. Electron-dense domains (condensed phase) were located on top of regions of
329 negative membrane curvature, and were surrounded by a less electron-dense phase (dilute phase)
330 associated with regions of positive membrane curvature (Fig. 2, col. 5). After primexine phase
331 separation was completed, probacula (sites of sporopollenin accumulation) began forming on the
332 plasma membrane, between electron-dense regions of primexine material and on regions of
333 positive membrane curvature (Fig. 2, col. 5, circled). A dilute phase of primexine can also be
334 observed between the pools of the denser phase in an image of tetrad pollen with a broken
335 callose wall but no enzymatic digestion (Fig. 2, col. 5). The final, sixth stage shows the mature
336 pollen grain with the exine fully deposited onto the patterned primexine; the final exine pattern is
337 formed from the template of low-density primexine material formed during phase separation
338 (Fig. 2, col. 6). While the cytoskeleton is visible in regions of our TEM images, there was no
339 apparent spatial correlation between the location or organization of cytoskeletal elements and the
340 development of membrane undulations, or to the final observed pollen pattern.

341

342 *Primexine composition*

343   The glycosyl composition and linkage analysis of primexine material prepared from
344 developing *Passiflora incarnata* pollen showed a polysaccharide material formed from linkages
345 of a complex mixture of monosaccharides. Given the small amount of material (112.2 μg) we
346 were able to isolate, it was not possible to characterize in detail the chemical structure of the
347 original primexine material. Signal to noise in this analysis was further degraded due to the fact
348 that whole cells were analyzed, such that ~95% of the total residues present were unlinked
349 glucose monomers, and therefore very likely from the cytoplasmic energy stores, not the
350 extracellular matrix. The remaining 5% of residues represented a wide variety of
351 monosaccharides. Several residues, notably galactose (Gal) and mannose (Man), were linked at
352 multiple sites within the monosaccharide, suggesting that the parent material was highly
353 branched. Therefore, after normalizing for glucose content, the constituent monosaccharides and
354 their linkages present during pollen pattern formation were broadly consistent with a mixture of
355 highly branched cellulose, pectin, and hemicellulose-like polymers. The full analysis is available
356 in the supplemental data.

357

358 *Phase Diagram Exploration*

359   To better understand the landscape of patterns generated by this physical mechanism, we
360 explored the equilibrium phase space of the effective Hamiltonian in Eq. (6) by finding the
361 minimum energy states for a range of parameter values. A rich pattern space resulted just from
362 tuning the two dimensionless parameters l_0 and $\lambda_3{}'$ and setting $R^2\tau/K = -1$. Much of this
363 phase space was comprised of patterns with spikes and holes in various polyhedral arrangements;
364 several examples are shown in Figure 3. We found that these patterns could often be categorized
365 into one of three general symmetric types: regular and modified polyhedral spikes; their inverses

12

366   (duals), in which the spikes become holes; and chiral stripes (Fig. 3). Chiral stripes were only
367   observed when $\lambda'_3 = 0$ and l_0 was a half integer value (consistent with observations by Sigrist
368   and Matthews)[41]. Chiral stripes have parity symmetry with two chiralities that are energetically
369   degenerate; this degeneracy may be broken by higher-order chiral terms as shown by
370   Dharmavaram and colleagues, thereby biasing a single chirality[17]. These higher-order terms may
371   also plausibly generate the more straight stripes observed in the pollen grains. When this
372   categorization of simple polyhedra or chiral stripes did not apply, the pattern typically
373   represented a mixture of two simpler polyhedral types and/or chiral stripes. Note that for $l = l_0$
374   states with odd l_0, the Gaunt coefficient in front of λ'_3 vanishes, so the pattern has no λ'_3
375   dependence in that case. For even values of l_0, the sign of λ'_3 determined whether the pattern
376   consisted of spikes or holes. At $\lambda'_3 = 0$, the spike and hole patterns are degenerate due to the
377   $\psi \to -\psi$ symmetry in the energy. We found that in some regions, the phase space had
378   boundaries across which discontinuous pattern changes were observed (solid lines in Fig. 3). In
379   other regions, patterns gradually changed with systematic tuning of parameters (Fig. 3). We note
380   that we were interested in the broad features of the phase diagram, not the specific characteristics
381   of the phase transitions between patterned states, such as how their continuous or discontinuous
382   nature might change if we include, for example, thermal fluctuations[14,42] or contributions from
383   modes away from $l = l_0$. Finally, we note that in our analysis we found that local minimum
384   states for a given parameter set could match the global minimum state for a separate parameter
385   set (corresponding to areas of coexistence). The occurrence and complexity of these global and
386   local minima is in marked contrast to the planar geometry, where just three stable patterns are
387   observed regardless of the pattern wavelength: uniform stripes, hexagons, or inverted
388   hexagons[43]. Our results are intuitive because on a sphere, none of these three planar patterns can
389   fully wrap the sphere without introducing defects (e.g, pentagonal arrangements of holes and
390   spikes, or points where the stripes collide or end); the many possibilities for accommodating
391   defects yield more possibilities for producing minima in the free energy, as observed in the
392   complexity we find in our phase diagram.
393   In studying the dynamics of our model, we found that conserved dynamics indeed yield
394   foamy structures at finite times, as expected from the flat 2d geometry case[34] (Fig. 1, red box).
395   These structures are not identical when different initial conditions are used, so we would
396   generally expect a range of disordered structures in pollen grains of a given non-equilibrating
397   species. We corroborate this prediction with a field of pollen from a single species (*Passiflora*
398   *incarnata*), which demonstrates that different foamy pollen grains of the same species are
399   slightly different, with a distribution of similar wavelengths comprising the overall reticulate
400   pattern (Fig. 2, col. 5).
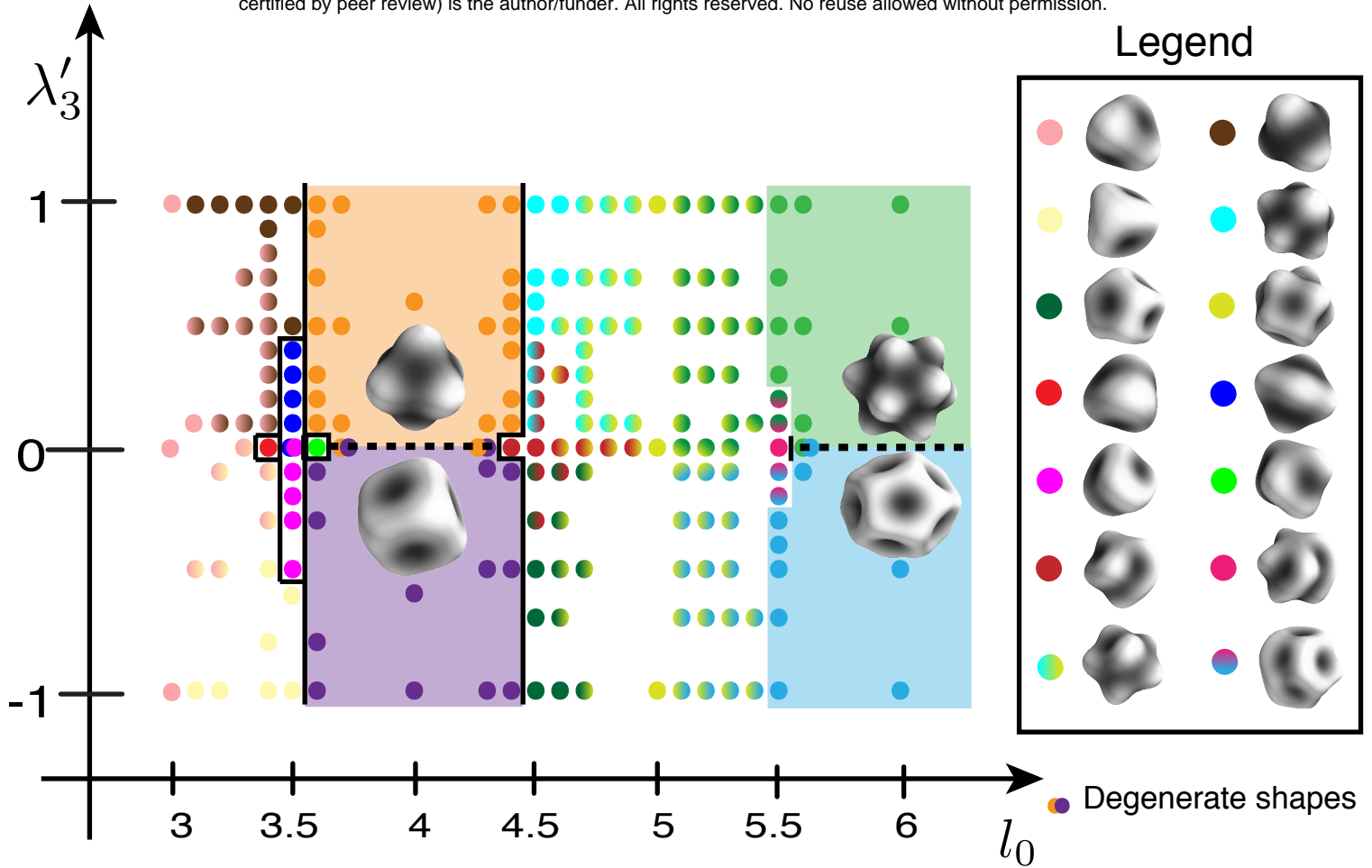
Figure 3: Phase Diagram of Simulations at Equilibrium. Calculated energy minima in the (l_0, λ_3') plane at equilibrium (Eq. 6). Each calculated point is color-coded according to the geometry of the minimum energy state found at that point in the space. Chiral stripe geometry is found at equilibrium when l_0 is a half integer and λ_3'=0. The rest of the space contains polyhedral spike patterns and their inverses. The boundaries between distinct pattern geometries are indicated by black lines. For example, there is a boundary line between l_0=3.5 and l_0=3.6 from λ_3'= 0.1 to λ_3'=1.0 across which we observe a discontinuous change in the pattern formed at equilibrium. In contrast, in other regions of the diagram, such as between l_0=4.5 and l_0=5.5 for λ_3'=1.0, there is a gradual transition in geometry from one minimum energy state to the next without a distinct boundary line. The legend shows the geometric patterns that correspond to a given color in the phase space. Overlapping dots represent degenerate states. Dots with a gradient of two colors represent intermediate states that are mixtures between two states. Colored shading represents large regions of the space with a single symmetrical pattern.

Evolutionary Trait Reconstruction

401
402   We matched patterns generated by our theory to those observed in a pollen database;
403   when we restricted our analysis to monads with documented membrane undulation during
404   development, our dataset represented ~45% of the 453 described families in Sporophyta. This is
405   a minimum set of families potentially described by our theory, since not all families have
406   described pollen and our theory also likely applies to non-monad pollen. This analysis showed
407   that only 27 of 202 included families contain species whose pollen patterns are consistent with
408   an equilibrium state (Fig. 4). Only seven of those 27 families contain species with pollen patterns
409   solely in equilibrium states. The remaining 175 families consist of species exhibiting only non-
410   equilibrated patterns. We found that equilibrium patterns are present throughout angiosperms,

14

411 including in gymnosperms, monocots, and eudicots. Notably, equilibrium patterns were absent
412 from the Magnoliids and five other basal families with intermediate branch order between
413 gymnosperms and angiosperms. In gymnosperms, only Welwitschiaceae and Ephedraceae had
414 species with equilibrium pattern states, and both patterns were striped. In monocots, Araceae and
415 Iridaceae had some species with equilibrium patterns, consisting of stripes and polyhedral tiling,
416 respectively. All species in the family Alismataceae had an equilibrium pattern with a polyhedral
417 distribution of pore-like apertures. The rest of the families with some equilibrium states were
418 found in eudicots; their surface patterns were **stripes** (Rubiaceae, Boraginaceae,
419 Scrophulariaceae, Sarraceniaceae, Primulaceae, Lentibulariaceae, Polygalaceae, Acanthaceae,
420 Berberidaceae), **polyhedral spikes** (Asteraceae, Zygophyllaceae, Amaranthaceae,
421 Cucurbitaceae, Alismataceae, Cactaceae, Convolvulaceae, Caryophyllaceae, Polygonaceae,
422 Buxaceae, Polemoniaceae, Martyniaceae, Euphorbiaceae), and **polyhedral holes**
423 (Polemoniaceae, Buxaceae, Polygonaceae, Convolvulaceae, Nyctaginaceae, Zygophyllaceae).
424 Some families had both polyhedral spike and polyhedral hole patterns because the polyhedral
425 arrangement of their apertures fit into a larger exine pattern (see Fig. 1, Convolvulaceae). Of
426 these, only four families contained species with only equilibrated patterns: Polygalaceae,
427 Amaranthaceae, Nyctaginaceae, and Martyniaceae. Examples of each of the pattern types can be
428 found in Figure 1 and the supplemental information.

429 **Table 1: Model Rates and Probabilities**

Model	No. rates	$-\ln L$	Transition rates	Probability of root state	States
2-state eq. model	2	31.850555	qAB = 94.0 qBA = 4.48	P(A)=0.500 P(B)=0.500	A: at eq. B: not at eq.
Null model for eq. model	1	34.454052	qAB=qBA =0.235	P(A)=0.997 P(B)=0.00285	
3-state λ model	6	125.18975	qED=29.7 qEC=0 qDE=68.1 qDC=23.2, qCE=58.8, qCD=0	P(C)=P(D) =P(E)=0.333	
Coarser/finer λ model	2	125.39324	qED=qEC=qDC=22.2, qDE=qCE=qCD=100	P(C)=P(D) =P(E)=0.333	C: λ > 3μm D: 1> λ >3μm E: λ < 1μm
Null model for λ model	1	137.01527	qED=qEC=qDC=qDE=qCE=qCD=0.942	P(C)=0.135, P(D)=0.111, P(E)=0.754	

430 **Table 2: Hypothesis Tests**

Models compared	Likelihood ratio	DOF	p-value	Kept model
2-state eq. vs null	5.21	1	0.05-0.01	2-state eq.
3-state λ vs null	23.7	5	<<0.01	3-state λ
3-state λ vs coarser/finer	0.407	4	0.99-0.95	coarser/finer
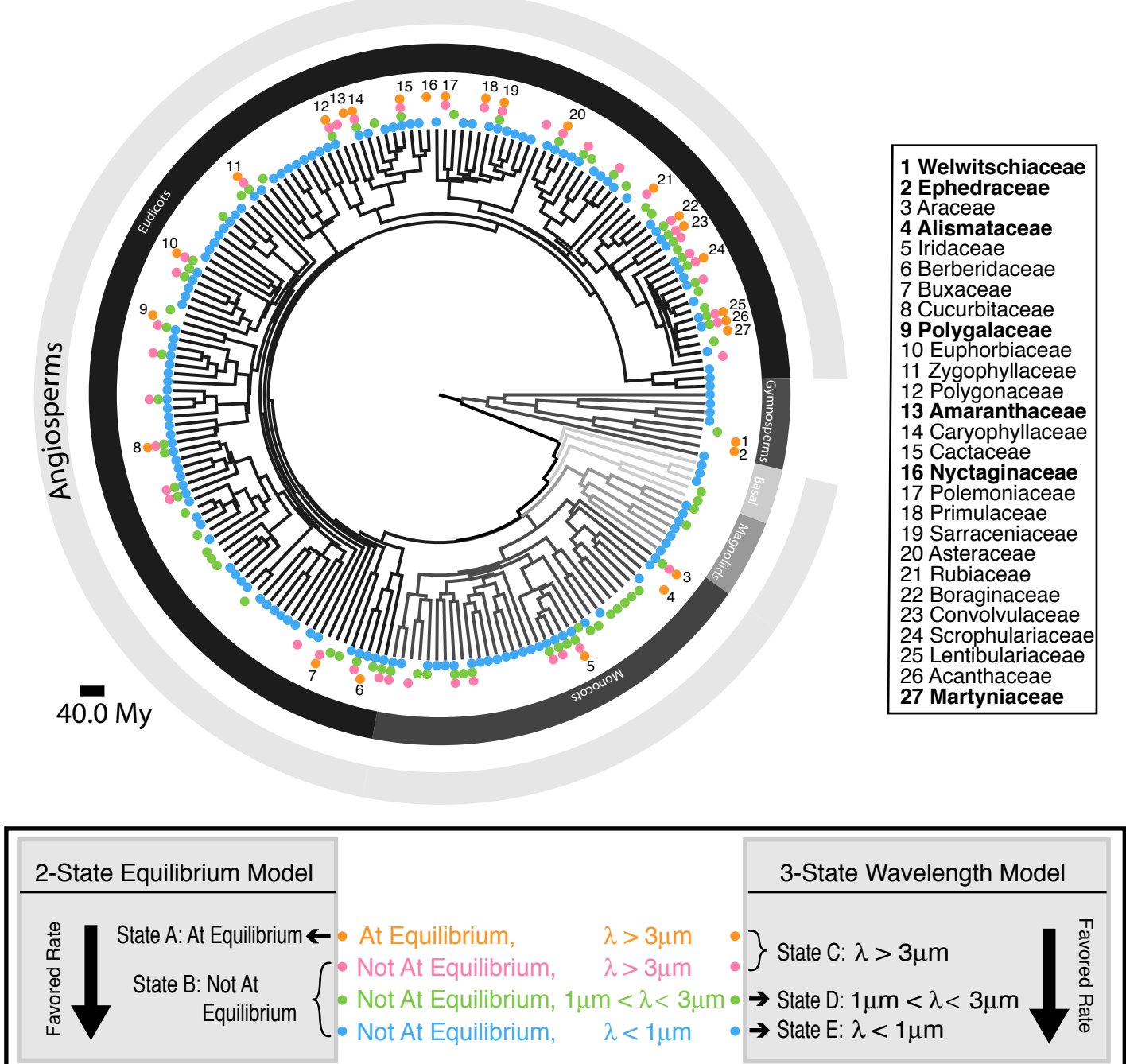
Figure 4: Angiosperm Phylogenetic Tree with Character States. Top panel: Phylogenetic tree of spermato-phytes with 202 families at terminal taxa. Colored dot represent the character states of the species within each family. Each terminal taxon is labeled with up to four states. The numbered families (27 in total) are those that have species that are in an equilibrium states. The families listed in black have more than one state; families listed in bold (seven of the 27) only have species that are in an equilibrium state. **Bottom panel:** legend for tree and description of categorization of states for two evolutionary models tested. We find that the favored rates are towards not at equilibrium patterns and smaller wavelengths. The scale bar represents 40.0 million years.

16

433   We initially hypothesized that if different pollen patterns served different
434 ecophysiological functions, evolution would select for patterns that reach equilibrium during
435 development, since this is presumably a more developmentally predictable and replicable state.
436 We tested this hypothesis using two models of ancestral state reconstruction: a 2-state
437 equilibrium model and a 3-state wavelength model. In the 2-state equilibrium model, we binned
438 our four identified pattern categories of wavelength and equilibrium (see methods) into two
439 evolutionary states, A and B, such that state A is all patterns at equilibrium and state B is all
440 patterns not at equilibrium (Fig. 4, bottom panel). The log-likelihood ratio of the 2-state
441 equilibrium model compared to the null model (where both rates are equal) was 5.21, so with one
442 degree of freedom, the p-value was between 0.01 and 0.05 (Table 2). We therefore reject the null
443 model and find that the rate of evolutionary transition from equilibrium to non-equilibrium
444 patterns is ~20-fold greater than the reverse rate (Table 1, qAB=94.0, qBA = 4.48). We also
445 found that the state at the root of spermatophytes had equal probability of being at equilibrium or
446 non-equilibrium.
447   We then tested the 3-state wavelength model by re-sorting categories (1)–(4) so that state
448 C represented all patterns with wavelengths greater than 3 μm, state D represented patterns with
449 wavelengths between 1 and 3 μm, and state E represented patterns with wavelengths less than 1
450 μm (see methods and Fig. 4, bottom panel). We first compared the 3-state wavelength model to
451 the null model and found a likelihood ratio of 23.7 given five degrees of freedom, for a p-value
452 <<0.01. Therefore, we reject the null hypothesis and accept the 3-state wavelength model. We
453 next compared the 3-state wavelength model with a simpler coarser/finer model where we
454 restricted all rates towards larger wavelengths (coarser) to be equal to each other (Table 1,
455 qED=qEC=qDC) and all rates towards smaller wavelengths (finer) to be equal to each other
456 (Table 1, qDE=qCE=qCD). The likelihood ratio between these two models resulted in a p-value
457 between 0.99 and 0.95, such that there was no significant difference between them. It is
458 therefore likely to be the case that pollen evolves more rapidly from equilibrated polygonal
459 patterns to finely reticulated or bumpy patterns than the reverse, and that any more complicated
460 model of pattern type evolution will be over fit. In other words, evolution seems to favor pollen
461 that never reaches equilibrated patterns, and similarly, foamy (reticulate) or unpatterned pollen
462 seems favored over the more interesting-to-humans pollen with well-defined polygonal patterns.
463
464 **Discussion**
465   We observed that both the electron density and the surface distribution of the primexine of
466 *Passiflora incarnata* change, becoming inhomogeneous, during pattern development. Because
467 the primexine electron density is initially uniform but subsequently separates into two distinct
468 electron densities, primexine development is consistent with a phase separation into a dense and
469 a dilute phase. The phase transition of polysaccharide materials of this kind is expected in the
470 absence of cross-linking factors (perhaps, for example, into phases with more- and less-branched
471 polymers). Additionally, we observed that the denser phase correlates to the plasma membrane
472 undulations (with discrete patches of dense material sitting inside the dips in the membrane).

17

473 Therefore, our data suggest that the more dense primexine regions cause the plasma membrane
474 to curve away from its initially featureless, spherical shape. The final pollen exine pattern is then
475 negatively templated by the pooled dense primexine and correlated membrane curvature.

476   A previous study of *Brassica campestris* pollen, another reticulate species, also demonstrated
477 the same deposition of primexine on the plasma membrane surface[44] followed by plasma
478 membrane undulations correlated to a dense primexine phase. In addition to the many reticulate
479 species whose patterns seem to be templated by plasma membrane undulations, species with
480 other surface patterns such as the polygonal holes of *Ipomoea purpureae*[45] or the polygonal
481 spikes of *Farfugium japonicum*[46] also exhibit early membrane undulations at the same
482 wavelength as the mature pattern features. However, primexine was not preserved in these
483 studies[23].

484   Although we were unable to determine the exact chemical composition of the primexine, the
485 constituent monosaccharides and their linkages are consistent with a mixture of cellulose, pectin-
486 and hemicellulose-like polysaccharides. Mixtures of different polysaccharides tend to phase
487 separate unless a cross-linker actively prevents them from demixing[26], such that phase separation
488 of primexine material on the surface of a developing pollen cell is perhaps not surprising.

489   Our theory shows that this phase separation of a material on the surface of a spherical cell,
490 when coupled to membrane elasticity (i.e., membrane buckling), yields an effective free energy
491 that exhibits spatially modulated phases. This effective free energy, using both single-mode and
492 two-mode approximations, produced equilibrium states corresponding to a variety of spikes,
493 holes, and chiral stripes on the surface of a sphere. These equilibrium patterns generated by our
494 theory also correspond to about ten percent of the pollen patterns documented in PalDat. We
495 expect that other highly ordered, patterned pollen may also fit our model when we include more
496 modes.

497   The more disorganized patterns observed in ~90% of analyzed species may be explained
498 by the dynamics of the process encoded by our model. Indeed, if we arrest the dynamics after
499 some short time (before equilibrium can occur), we find states that resemble the foamy, more
500 disordered pollen structures. In the planar case, some of these foamy structures may even be
501 relatively stable, as discussed in more detail by Guttenberg and colleagues[34]. Applying the
502 techniques in this work to the surface of a sphere would be an interesting topic for future
503 research.

504   Given the observation of so many species that either have a non-equilibrated pattern, or
505 no pattern at all, it is worth thinking about what this means in the context of our general physical
506 theory. One possibility is that most plant materials have effective free energy parameters that
507 barely favor phase separation of the primexine. This possibility would explain both the repeated
508 evolution of featureless pollen and the high abundance of disordered structures, both of which
509 could result from the slower kinetics and enhanced fluctuations that one would generally expect
510 near a phase transition, especially if the phase transition has only a weakly discontinuous
511 character. In mixtures that start near such a critical point, small variations of the parameters
512 (induced, for example, by small changes in chemical composition of the primexine) could induce
513 large changes in the patterning. This possibility might lend additional weight to our physical
514 theory as an explanation of the observed pattern diversity; small evolutionary shifts in primexine

18

515 composition could fundamentally alter the mature pollen pattern, leading to the relatively large

516 shifts in pollen patterns in short periods of time that have demonstrably occurred in evolution.

517 Although we did not detect an elevated rate of appearance of equilibrium patterns, the tree is

518 consistent with many instances of equilibrium pollen patterns arising from evidently non-

519 equilibrium patterns of recent ancestors. For example, the families Asteraceae, Sarraceniaceae,

520 and Cactaceae all exhibit equilibrated patterns that are nested in clades in which the other

521 families exhibit only non-equilibrated patterns. Another possible explanation for the prevalence

522 of the disordered states is that primexine phase separation is typically arrested by sporopollenin

523 deposition before it can bring the pollen grain into an equilibrium pattern. In addition, cross-

524 linkers such as calcium ions are often found in plant cell walls, the presence of which might also

525 contribute to the formation of the more disordered patterns by arresting the underlying separation

526 dynamics.

527   After classifying extant pollen patterns as either equilibrium states versus kinetically

528 arrested or generally disordered patterns, both of which are predicted by the physical mechanism

529 proposed here, we conclude from an evolutionary analysis that the highly ordered patterns for

530 which pollen are famous have not arisen under strong selection. In fact, our results are more

531 consistent with an evolutionary bias toward unpatterned, typically foamy (reticulate) states. This

532 evolutionary result is also consistent with our physical picture, since the constituents of the

533 primexine are naturally phase-separating compounds and should induce the patterning without

534 any additional biological control. So, perhaps the exine patterns that give pollen their fascinating

535 variety do not serve any particular purpose, but are rather a natural consequence of the

536 composition of the primexine and simple physical principles.

537   There is much room for future work. Our theory, and its apparent reification in pollen

538 development, describe a novel and robust mechanism for repeatedly patterning surfaces at both

539 micron and nanometer scales. Therefore, it would be of basic interest to materials science to

540 understand how to program the general parameters of our theory in polymer chemistry. By fully

541 characterizing the primexine material, it would be possible to study its phase properties and their

542 contribution to the pattern-governing parameters in our model. Finally, in contrast to the

543 currently employed pollen descriptive scheme of overlapping categories of unit, polarity,

544 aperture, ornamentation, and wall structure, nearly all unique pollen patterns can be fully

545 recapitulated by a unique set of parameters in our Hamiltonian (eq. 6). It may be useful in the

546 future to describe pollen species by these unique energetic parameters; this scheme also has the

547 advantage that these energetic parameters will ultimately map to the biochemistry and timing of

548 pollen development.

549

Acknowledgements

19

References

1. Blackmore, S., Wortley, A.H., Skvarla, J.J., & Rowley, J.R. Pollen wall development in flowering plants. *New Phytol.* **174**, 483-498 (2007)

2. Locke, M. *Microscopic Anatomy of Invertebrates*. Eds Harrison FW, Locke M (Wiley-Liss, New York) **11A**, 75–138 (1998)

3. Ariizumi, T. & Toriyama, K. Genetic regulation of sporopollenin synthesis and pollen exine development. *Annu Rev Plant Biol.* **62**, 437–460 (2011)

4. Blackmore, S. & Crane, P.R. The evolution of apertures in the spores and pollen grains of embryophytes. *Rep Biol.* 159-182 (1998)

5. Katifori, E., Alben, S., Cerda, E., Nelson, D.R., & Dumais, J. Foldable structures and the natural design of pollen grains. *PNAS* **107**, 7635-7639 (2010)

6. Owen, H.A. & Makaroff, C.A. Ultrastructure of microsporogenesis and microgametogenesis in *Arabidopsis thaliana* (L.) Heynh. ecotype Wassilewskija (Brassicaceae). *Protoplasma.* **185**, 7-21 (1995)

7. Nishikawa, S., Zinkl, G.M., Swanson, R.J., Maruyama, D., & Preuss, D. Callose (β-1,3 glucan) is essential for *Arabidopsis* pollen wall patterning, but not tube growth. *BMC Plant Biol.* **5**, 22 (2005)

8. Heslop-Harrison, J. Tapetal origins of pollen-coat substances in Lilium. *New Phytol.* **67**, 779-786 (1968)

9. Skvarla, J.J. & Larson, D.A. Fine Structural Studies of Zea mays Pollen I: Cell Membranes and Exine Ontogeny. *Am J Bot.* **53**, 1112-1125 (1966)

10. Godwin, H., Echlin, P., & Chapman, B. The development of the pollen grain wall in *Ipomoea purpurea* (L.) Roth. *Rev. Palaeobot. Palynol.* **3**, 181-195 . (1967)

11. Rowley, J.R. Germinal Apertural Formation in Pollen. *Taxon* **24**, 17-25 (1975)

12. Furness, C.A. A review of spiraperturate pollen. *Pollen et Spores* **27**, 307-320 (1985)

13. Albert, B., Nadot, S., Dreyer, L., & Ressayre, A. The influence of tetrad shape and intersporal callose wall formation on pollen aperture pattern ontogeny in two eudicots species. *Ann. Bot.* **106**, 557-564 (2010)

14. Lavrentovich, M.O., Horsley, E.M., Radja, A., Sweeney, A.M., & Kamien, R.D. First-order patterning transitions on a sphere as a route to cell morphology. *PNAS*. **113**, 5189-5194 (2016)

15. Leibler, S. & Andelman, D. Ordered and curved meso-structures in membranes and amphiphilic films. *J Phys*. **48**, 2013–2018 (1987)

16. Dharmavaram, S., Xie, F., Klug, W., Rudnick, J., & Bruinsma, R. Landau theory and the emergence of chirality in viral capsids. *EPL* **116**, 26002 (2016)

17. Dharmavaram, S., Xie, F., Klug, W., Rudnick, J., & Bruinsma, R. Orientational phase transitions and the assembly of virus capsids. *Phys. Rev. E*. **95**, 062402 (2017)

18. Andelman, D., Kawakatsu, T., Kawasaki, K. Equilibrium shape of two-component unilamellar membranes and vesicles. *Europhys. Lett.* **19**, 57-62 (1992)

19. Taniguchi, T., Kawasaki, K., Andelman, D. and Kawakatsu, T. Phase transitions and shapes of two component membranes and vesicles II : weak segregation limit. *J. Phys. II France*. 4, 1333-1362 (1994)

20. Zhang, L., Wang, L., & Lin, J. Defect structures and ordering behaviours of diblock copolymers self-assembling on spherical substrates. *Soft Matter*. **10**, 6713–6721 (2014)

21. Sannier, J., Baker, W.J., Anstett, M.C., & Nadot, S. A comparative analysis of pollinator type and pollen ornamentation in the Araceae and the Arecaceae, two unrelated families of the monocots. *BioMed Central*. **2**, 145 (2009)

22. Furness, C.A. & Rudall, P.J. Pollen aperture evolution – a crucial factor for eudicot success? *Trends in Plant Sci*. **9**, 154-158 (2004)

23. Gabarayeva, N.I. & Grigorjeva, V.V. Exine development in *Stangeria eriopus* (Stangeriaceae): ultrastructure and substructure, sporopollenin accumulation, the equivocal character of the aperture, and stereology of microspore organelles. *Rev. Palaeobot. Palynol*. **122**, 185-218 (2002)

24. Kirkpatrick, A.B. & Owen, H.A. Observation of early pollen exine patterning by scanning electron microscopy. *Microsc. Microanal*. **19**, 134-135 (2013)

25. Santander, J. *et al*. Mechanisms of intrinsic resistance to antimicrobial peptides of *Edwardsiella ictaluri*and its influence on fish gut inflammation and virulence. *Microbiology*. **159**, 1471-1486 (2013)

26. Tolstoguzov, V. Phase behavior in mixed polysaccharide systems. *Food Polysaccharides and Their Applications 2nd ed.* Eds. Stephen AM, Phillips GO, Williams PA. Boca Raton: Taylor & Francis 589-627 (2006)

27. Kim, S. & Willett, J. L. Isolation of amylose from starch solutions by phase separation. *Starch*. **56**, 29-36 (2004)

28. Abramowitz, M. & Stegun, I.A. *Handbook of Mathematical Functions* (National Bureau of Standards, Washington, DC) (1972)

29. Johansson, H.T. & Forssén, C. Fast and accurate evaluation of Wigner 3j, 6j, and 9j symbols using prime factorisation and multi-word integer arithmetic. ArXiv: 1504.08329 (2015)

30. Kamien, R.D. The geometry of soft materials: A primer. *Rev Mod Phys*. **74**, 953–971. (2002)

31. Press, W.H., Teukolsky, S.A., Vetterling, W.T., & Flannery, B.P. *Numerical Recipes : the Art of Scientific Computing*. Cambridge [Cambridgeshire]: Cambridge University Press (1986)

32. Elder, K.R., Katakowski, M., Haataja, M., & Grant, M. Modeling Elasticity in Crystal Growth. *Phys Rev Lett*. **88**, 245701 (2002)

33. Guyer, J.E., Wheeler, D., & Warren, J.A. FiPy: Partial Differential Equations with Python. *Comput Sci Eng*. **11**, 6-15 (2009)

34. Guttenberg, N., Goldenfeld, N. & Dantzig. J. Emergence of foams from the breakdown of the phase field crystal model. *Phys. Rev. E*. **81**, 065301 (2010)

35. PalDat – a palynological database (2000 onwards, www.paldat.org), downloaded on 9/27/16)

36. Weber, M., Halbritter, H., & Hesse, M. The spiny pollen wall in Sauromatum (Araceae) – with special reference to the endexine. *Int. J. Plant Sci*. **159**,744-749 (1998)

37. Harris, L. W., Jonathan Davies, T. A Complete Fossil-Calibrated Phylogeny of Seed Plant Families as a Tool for Comparative Analyses: Testing the 'Time for Speciation' Hypothesis. *PLoS ONE*. **10**, e0162907 (2016)

38. Hinchliff, C. E. *et al*. Synthesis of phylogeny and taxonomy into a comprehensive tree of life. *PNAS*. **112**, 12764-12769 (2015)

39. Pagel, M., Meade, A., 2006. BayesTraits. Available from: <http://www.evolution.rdg.ac.uk/BayesTraits.html>.

40. Pagel, M. The Maximum likelihood approach to reconstructing ancestral character states of discrete characters on phylogenies. *Syst Biol*. **48**, 612-622 (1999)

41. Sigrist, R., Matthews, P. Symmetric spiral patterns on spheres. *SIAM J Appl Dyn Syst*. **10**, 1177–1211 (2011)

42. Brazovskii, S.A. Phase transition of an isotropic system to a nonuniform state. *J Exp Theor Phys*. **68**,175-185 (1975)

43. Brazovskii, S.A., Dzyaloshinskii, I.E., & Muratov, A.R. Theory of weak crystallization. *J Exp Theor Phys*. **66**, 625-633 (1987)

44. Fitzgerald, M.A. & Knox, R.B. Initiation of primexine in freeze-substituted microscpores of *Brassica campestris*. *Sex plant reprod*. **8**, 99-104 (1995)

45. Takahashi, M. Development of the echinate pollen wall in *Farfugium japonicum* (Compositae: Senecionea). *Bot. Mag*. **102**, 219-234 (1989)